Effect of Boron on the Oxidation Behavior of NiCrAlYHfTi in H_2O and CO_2 Environments

K. A. Unocic, D. N. Leonard and B. A. Pint
Materials Science and Technology Division
Oak Ridge National Laboratory, Oak Ridge, TN 37831 USA

Cast NiCrAl alloys, co-doped with Y, Hf, Ti, and/or B, were evaluated at 1100°C and 1150°C in dry air, wet air (10 or 50% H_2O), and CO_2-10%H_2O, in order to study the effect of boron additions on alumina scale growth and adhesion. After 200 cycles at 1100°C, all of the alloys with Y and Hf showed good scale adhesion. **By increasing the test temperature to 1150°C, the addition of ~0.3 at.% (0.07 wt.%) B was shown to improve alumina scale adhesion during 1-h cycles in air with 10%H_2O.** Analytical transmission electron microscopy showed no effect of B on the alumina scale microstructure and only minor effects on the depth of internal oxidation at 1100°C. Combined Ti and B additions did not produce an additional benefit and **Cr-B precipitates were detected in both B-doped alloys**. Exposures in O_2-buffered CO_2-H_2O did not result in any detrimental effect at 1100°C.

Keywords: NiCrAl, water vapor, CO_2, Reactive Elements, α-Al_2O_3, Boron

Introduction

Bond coatings are an integral part of a thermal barrier coating (TBC) system [1] and the growth and adhesion of the thermally-grown alumina scale can be a key to their high temperature performance. It is widely recognized that reactive element (RE) additions (e.g. Y, Hf, Zr, La, Ce) play a major role in the adhesion and growth of alumina scales [2-4] and that RE co-doping provides the best performance in laboratory alloys [5-8], commercial alloys and bond coatings [5,9-13]. However, a direct comparison of NiCoCrAlY bond coatings with and without Hf and Si additions showed a **similar drop in TBC lifetime for both types of bond coatings** with the addition of water vapor in furnace cycle testing [13]. Thus, in the search for new bond coating solutions for coal-derived syngas-fired turbines for power generation [14-17], modifications beyond RE-doping were examined. In particular, the higher H_2O [17] and

possibly higher CO_2 contents in clean coal systems may require new coating solutions, which may assist in eliminating the de-rating (i.e. firing at a lower temperature, thereby reducing efficiency) of syngas-fired turbines [17].

Boron has long been known to have beneficial effects on the **mechanical properties of** superalloys [18] and is currently being studied for new Co-base superalloys [19]. It is also well-documented that B prevents the H embrittlement of Ni- [20] and Fe-base aluminides [21]. In addition, boron has been shown to improve the steam oxidation resistance of steels [22], where the injection of H into the alloy substrate is thought to negatively affect oxidation behavior in chromia-forming alloys [23] **and alumina-forming alloys including TBC adhesion [24,25]**. Boron has previously been considered as a beneficial bond coating additive [26,27]. **In this study, the high temperature cyclic oxidation behavior of cast model NiCrAl alloys was evaluated with combinations of Y, Hf, Ti and B as a first step in evaluating B as a bond coating addition.** The co-doping of Ti and B was done to simulate interdiffusion of Ti from the superalloy substrate into the bond coating [8,12,28] and to investigate the potential for TiB_2 formation [29,30]. In wet air cyclic testing at 1150°C, B additions in the alloys with Y and Hf were found to improve alumina scale adhesion.

Experimental Procedure

Model NiCrAl alloys were cast and homogenized (4h/1200°C in vacuum) with the compositions shown in Table 1 and all compositions given in at.%. Coupons with ~16mm diameter and 1-1.5mm thickness were polished to a 600 grit SiC (for cyclic tests) or 0.3 μm alumina (for isothermal tests) final finish and ultrasonically cleaned in acetone and methanol prior to exposures: (1) at 1100°C isothermal thermal gravimetric analysis (TGA) using a Cahn model 1000 microbalance and (2) at 1100° and 1150°C using 1h cycles with 10 min cooling between cycles using an automated system and weighing the specimens every 20 cycles on a Mettler-Toledo model XP205 balance with an accuracy of ±0.01 mg/cm^2. Four environments were used: dry air or O_2 (0% H_2O), air with 10 vol.% or 50% H_2O and 10%H_2O+90%(CO_2-0.15%O_2). The carbon activity in the latter environment was calculated to be 10^{-32}. **For all environments, at the end of each thermal cycle, gas flow was stopped and the specimens**

were cooled in laboratory air to prevent water condensation on the specimens. After exposure, specimens were characterized by scanning electron microscopy (SEM) (Hitachi model S3400 and S4800), scanning-transmission electron microscope (STEM) (Philips model CM200) operated at 200kV and equipped with a Schottky field emission gun (FEG) and x-ray energy dispersive spectrometer (EDS). For polished cross-sections, specimens were Cu-plated prior to sectioning. TEM specimens were prepared via the focus ion beam (FIB) in-situ lift-out technique using a Hitachi NB5000 FIB-SEM. Internal oxidation beneath the oxide scale was measured using approximately 40 measurements from the polished cross-sections using ImageJ software.

Results and Discussion

Figure 1a compares the cyclic oxidation behavior of the eight alloys in 4 different environments at 1100°C, showing the final mass change after 200, 1-h cycles. For the Y+Hf co-doped alloys, there was no effect of adding H_2O or CO_2 to the environment compared to dry air or O_2 with all of the alloys showing small mass gains and mostly adherent alumina scales. For the alloys without Hf, mass losses were typical, with the addition of H_2O generally increasing the mass loss as has been observed previously [8,31]. **These masses losses are small and reflect minor spallation, which increased with the addition of Ti and was not strongly affected by the addition of B, Figure 1a.** This spallation cannot be attributed to indigenous sulfur [32] as all of the alloys had low sulfur contents, Table I, **and the Y/S ratios were >>1 [33].** The one exception to the mass losses for alloys without Hf was the alloy with Y and B in air with 50%H_2O, where a mass gain was observed after 200 cycles and no spallation was apparent. As was observed previously [8], the addition of ~0.3%Ti had little effect on the mass change behavior. For the alloys with Hf that nominally formed an adherent oxide during this exposure, parabolic rate constants were fit to the mass gain data and compared to isothermal TGA data at 1100°C in Figure 1b. In most cases, the rate constants measured from the cyclic mass gain data were higher than those measured isothermally. The isothermal rate constants measured in CO_2-H_2O were consistently near 5 x 10^{-13} g^2/cm^4s, somewhat lower than those measured in dry air (6-9 x 10^{-13} g^2/cm^4s). More scatter in the rate constants was observed in air+10%H_2O. Previously it was noted that thinner oxides formed on

MCrAlY bond coatings oxidized in reducing Ar-H_2-H_2O environments [34]. **As reducing or low pO_2 conditions are not expected in a combustion turbine, the CO_2 contained 1500ppm O_2, which set the O_2 partial pressure in this condition.**

Rather than running longer times at 1100°C **to differentiate behavior**, additional experiments were conducted at 1150°C. Figure 2 shows the mass gain data for exposures out to 500, 1-h cycles. As at 1100°C, the **scales on** alloys with only Y or Y+Ti spalled quickly and the addition of B with only Y did not provide any benefit. The strongest benefit of B was for the alloys with Y and Hf where higher mass gains were observed for the alloys with B. The peak mass gain for the Y+Hf alloy without B was at ~150 cycles while spallation **(the onset of mass loss)** did not start until ~400 cycles for the alloy with Y, Hf and B. A second specimen was run to confirm this result. For the alloys with Y, Hf and Ti, there was only a small benefit of adding B–an offset of <100 cycles in the peak mass gain.

Characterization was performed on the alloys to determine if there were any microstructural effects due to the B additions. Figure 3 shows cross-sections of the YHfTi and YHfTiB-**doped** alloys exposed at 1100°C. The light microscopy images show the γ´ and β (darker) phases in the alloy and the Z-contrast SEM backscattered images show the alumina scale and internal oxidation, highlighting the brighter Hf-rich internal oxidation. Figures 3a-3d show specimens exposed in dry air, but no effect of B was evident in the scale morphology, the extent of internal oxidation or the β-depletion behavior. The Z-contrast of the SEM backscattered electron (BSE) images highlights the internally oxidized Y and Hf. As a comparison with the previous study [8], Figure 4 quantifies the internal oxidation after 200, 1-h cycles in environments without water vapor. The boxes are defined by the 25% and 75% values with the mean as the center line and the whiskers mark the maximum and minimum measurements. Unfortunately, the B containing alloys also had lower Y contents **compared to the alloys without B** (Table 1) so the slightly reduced internal oxidation observed in the B containing alloys may be attributed to this difference, Figure 4. As was observed previously [8], co-doped Y+Hf alloys showed less internal oxidation than the alloys with Y and Y+Ti and the addition of Ti reduced the **depth of** internal oxidation in each case. Figures 3e-3h show cross-sections of the alloy with Y, Hf, Ti and B after exposure in 10% and 50%H_2O. As was quantified previously [8], the internal oxidation increased with the addition of H_2O. Figures 3i and 3j

show cross-sections of the same alloy after exposure in the CO_2-H_2O environment, where no additional degradation (such as internal carburization) was observed as suggested by the mass change data in Figure 1.

Figure 5 shows representative cross-sections of specimens exposed at 1150°C for 200 cycles. **For the alloys without Hf, significant β depletion was observed reflecting the significant scale spallation for these alloys, Figures 5a and 5b. At higher magnification, Figure 5c shows the YHfB alloy with much less β depletion.** A third phase was identified rich in Cr and B, which is further discussed below. Figure 5d shows the same YHfB alloy exposed in air with 50%H_2O with a change in contrast to highlight these Cr-B precipitates. Figure 6 quantifies the internal oxidation observed in several of the alloys exposed for 200, 1-h cycles at 1150°C. Comparing the YHf and YHfB alloys, the internal oxidation was significantly reduced but this difference again could be due to the lower Y content in the B-containing alloy and perhaps due to the better scale adhesion on this alloy, Figure 2. Returning to the precipitates seen in Figures 5c and 5d, the precipitates were easier to image in Figure 5d and had an average size of 6.1±1.4 μm. As shown in Figure 7 for the alloys with Ti, similar precipitates were also observed in the YHfTiB alloy exposed at 1150°C (Figure 7d), but were not observed in the YHfTi alloy exposed at 1150°C (Figure 7c) or in corresponding specimens exposed at 1100°C (Figures 7a and 7b). Further characterization is needed to determine if this is due to coarsening at the higher temperature. After the 500, 1-h cycle exposure at 1150°C shown in Figure 7d, the precipitates were similar in size (5.9±1.7μm) but there appeared to be a ~250 μm precipitate depletion zone near the surface. Figure 8 shows EPMA maps from the center of the YHfTiB alloy exposed at 1150°C (shown in Figure 7d), where the precipitates were found to be primarily B and Cr. Auger electron spectroscopy also confirmed the precipitates to be rich in Cr and B. Further characterization did not find any Ti-rich precipitates or other indication of TiB_2 formation (a more stable boride) [29,30] at either temperature for the YHfTiB alloy. Both EPMA and x-ray diffraction data suggested that the precipitates are CrB [35] and Cr_3B_2, which also was predicted by thermodynamic calculations [36]. The depletion layer could suggest that B is participating in the reaction in some manner. The original research on beneficial B additions to aluminides [20,21] suggested a B-H interaction that has been shown to be very strong in a subsequent

study [37]. If B reacts with H in the alloy or at the metal-scale interface (injected by OH^- transport through the scale), this may counter any detrimental role of H. Assuming a B-H interaction, the depletion layer may suggest the depth to which H has penetrated. However, B has a low solubility in Ni-base alloys [38] and the depletion layer also may suggest that the benefit may be short-lived if B is needed at the metal-scale interface and if the B-rich reservoir phase is receding into the substrate.

In order to look for an effect of B on the alumina scale microstructure, TEM specimens were prepared, which complement the previous TEM work reported for the B-free model alloys [8]. Figure 9 shows STEM bright field (BF) images of the scale formed on the B-containing co-doped alloys after a 100h isothermal exposure at 1100°C in dry air. The inner α-Al_2O_3 has the typical columnar grain structure, interrupted by an internal oxide peg in Figure 9b. The outer Ni-containing oxide is variable in thickness, as shown in Figure 10a. As has been observed in numerous studies [5,39,40], pores were observed at or near the interface between the inner alumina layer and the outer, spinel-type oxide layer, suggesting a solid-state reaction between NiO and Al_2O_3 resulting in $NiAl_2O_4$ and voids that has been previously studied in detail [41]. In general, these scale microstructures were very similar to those observed on the B-free model alloys [8]. Also as observed previously [8], the **outer oxide layer** formed over the β-phase was thicker than the scale formed over the γ'-phase and mainly consisted of Cr and Al. The outer layer formed over the γ'-phase was thinner and had a slightly different appearance with equiaxed oxide grains containing Ni, no Y or Hf rich precipitates, and more voids at the **interface between the inner and outer oxide layers**. In the inner alumina layer, Y and Hf grain boundary segregation was detected similar to previous studies [5,8,11,12,40].

Returning to the effect of CO_2, **Figures** 10a and 10b show plan-view images of the scale formed on the alloy doped with Y, Hf and Ti after isothermal exposures at 1100°C in dry air and CO_2-H_2O, respectively. The outer transient oxide appeared to be thicker when the alloy was exposed to CO_2-H_2O, which may explain the slightly slower growth rate of the inner alumina layer in this environment, Figure 1b. Increased transient oxide formation also may be a concern for adhesion of the bond coating to the overlying ceramic top coating. STEM high-angle annular dark field (HAADF) images of the same specimens are shown in Figures 10c and 10d. These images also indicate that the transient, outer oxide

was thicker in the CO_2-H_2O environment. Otherwise, similar to comparisons made in dry and wet air, no major differences were noted when the scale was grown in the presence of CO_2. Since ~90%CO_2 did not appear to negatively affect scale growth **and** adhesion or TBC lifetime [42,43], it does not appear to be a concern for strategies to enrich CO_2 in turbine exhaust to facilitate carbon capture and storage.

Based on the possibility of a beneficial B effect on alumina scale adhesion in the presence of water vapor, B-containing powders have been atomized and bond coatings will be fabricated to determine if this benefit can lead to longer TBC lifetimes. In order to minimize B oxidation, a vacuum plasma spray **coating** process will be used for deposition.

Conclusions

The oxidation behavior of model NiCrAl alloys containing combinations of Y, Hf, Ti and B was investigated at 1100° and 1150°C in environments containing H_2O and CO_2. The **relatively** poor scale adhesion observed on alloys without Hf was not significantly improved by the addition of ~0.3B. For the adherent oxides formed on the alloys with Y and Hf at 1100°C, the addition of B did not change the oxidation performance in any of the environments investigated for 200 cycles. However, at 1150°C, the alloys containing B showed better scale adhesion, particularly for the alloy doped with Y, Hf and B compared to the alloy with only Y and Hf. The addition of B to the alloy did not appear to significantly affect the alumina **scale** microstructure or the depth of internal oxidation. At 1150°C, Cr-B precipitates were observed in the underlying substrate of the Y- and Hf-doped alloys containing B but were not observed after oxidation at 1100°C.

Acknowledgements

The authors would like to thank P. F. Tortorelli, H. Meyer, T. M. Lowe, G. W. Garner, T. Geer, T. Jordan and D.W. Coffey for assistance with the experimental work and for S. Dryepondt and M. P. Brady for comments on the manuscript. Research supported by the U.S. Department of Energy (DOE), Office of Coal and Power R&D in the Office of Fossil Energy, and by the Center for Nanophase Materials

Sciences (CNMS), which is sponsored by the Scientific User Facilities Division, DOE Office of Basic Energy Sciences.

References

[1] R. Darolia, Thermal barrier coatings technology: critical review, progress update, remaining challenges and prospects, Inter. Mater. Rev. 58(6) (2013) 315-348.

[2] B. A. Pint, Experimental Observations in Support of the Dynamic Segregation Theory to Explain the Reactive Element Effect, Oxid. Met. 45 (1996) 1-37.

[3] B. A. Pint, I. G. Wright, W. Y. Lee, Y. Zhang, K. Prüßner, K. B. Alexander, Substrate and Bond Coat Compositions: Factors Affecting Alumina Scale Adhesion, Mater. Sci. Eng. A 245 (1998) 201-211.

[4] J. Quadakkers, L. Singheiser, Practical Aspects of the Reactive Element Effect, Mater. Sci. Forum 369-372 (2001) 77-92.

[5] B. A. Pint, K. L. More, I. G. Wright, The Use of Two Reactive Elements to Optimize Oxidation Performance of Alumina-Forming Alloys, Mater. High Temp. 20 (2003) 375-386.

[6] B. A. Pint, Optimization of Reactive Element Additions to Improve Oxidation Performance of Alumina-Forming Alloys, J. Amer. Ceram. Soc. 86 (2003) 686-695.

[7] D. Naumenko, V. Kochubey, L. Niewolak, A. Dymiati, J. Mayer, L. Singheiser, W. J. Quadakkers, Modification of alumina scale formation on FeCrAlY alloys by minor additions of group IVa elements, J. Mater. Sci. 43 (2008) 4550-4560.

[8] K. A. Unocic, B. A. Pint, Oxidation Behavior of Co-Doped NiCrAl Alloys in Dry and Wet Air, Surf. Coat. Technol. 237 (2013) 8-15.

[9] J. T. DeMasi-Marcin, D. K. Gupta, Protective coatings in the gas turbine engine, Surf. Coat. Technol. 68-69 (1994) 1-9.

[10] T. Xu, S. Faulhaber, C. Mercer, M. Maloney, A. Evans, Observations and Analyses of Failure Mechanisms in Thermal Barrier Systems with Two Phase Bond Coats Based on NiCoCrAlY, Acta Mater., 52 (2004) 1439-1450.

[11] K. A. Unocic, B. A. Pint, Characterization of the Alumina Scale Formed on a Commercial MCrAlYHfSi Coating, Surf. Coat. Technol. 205 (2010) 1178-1182.

[12] K. A. Unocic, C. M. Parish, B. A. Pint, Characterization of the Alumina Scale formed on Coated and Uncoated Doped Superalloys, Surf. Coat. Technol. 206 (2011) 1522-1528.

[13] J. A. Haynes, K. A. Unocic, B. A. Pint, Effect of Water Vapor on the 1100°C Oxidation Behavior of Plasma-Sprayed TBCs with HVOF NiCoCrAlX Bond Coats, Surf. Coat. Technol. 215 (2013) 39-45.

[14] L. A. Ruth, Advanced clean coal technology in the USA, Mater. High Temp. 20 (2003) 7-14.

[15] N. A. H. Holt, Operating experience and improvement opportunities for coal-based IGCC plants, Mater. High Temp. 20 (2003) 1-6.

[16] B. M. White, R. W. Ames, P. Burke, Conditions in Advanced Turbines for IGCC Power Plants with Carbon Capture, ASME Paper #GT2013-94609, Proc. Turbo Expo 2013, 2013.

[17] I. G. Wright, T. B. Gibbons, Recent developments in gas turbine materials and technology and their implications for syngas firing, Int. J. Hydrogen Energy 32 (2007) 3610-3621.

[18] R. F. Decker, J. W. Freeman, Mechanism of beneficial effects of boron and zirconium on creep properties of complex heat-resistant alloy, Trans. Met. Soc. AIME, 218 (1960), 277-285.

[19] L. Klein, B. von Bartenwerffer, M.S. Killian, P. Schmuki, S. Virtanen, The effect of grain boundaries on high temperature oxidation of new γ´-strengthened Co–Al–W–B superalloys, Corros. Sci. 79 (2014) 29–33.

[20] C. T. Liu, C. L. White, J. A. Horton, "Effect of Boron on Grain Boundaries in Ni_3Al," Acta Met. 33 (1985) 213-229.

[21]. C. T. Liu, E. P. George, Environmental Embrittlement in Boron-Free and Boron-Doped FeAl (40 At.% Al) Alloys, Scripta Met. Mater. 24 (1990) 1285-1290.

[22] S. R. J. Saunders, J. A. Little, Improvements in the Adhesion and Protectiveness of Scales Formed on Iron-Chromium Steels By the Application of Boron Compounds, In: E. Lang, Editor, The Role of Active Elements in the Oxidation Behavior of High Temperature Metals and Alloys (Elsevier Applied Science, London, 1989) p.175-192.

[23] W. J. Quadakkers, J. Żurek, M. Hänsel, Effect of water vapor on high temperature oxidation of FeCr alloys, JOM 61 (7) (2009) 44-50.

[24] J. L. Smialek, "Moisture-Induced Delayed Spallation and Interfacial Hydrogen Embrittlement of Alumina Scales," JOM 58 (1) (2006) 29-35.

[25] J. L. Smialek, Moisture-Induced TBC Spallation on Turbine Blade Samples, Surf. Coat. Technol. 206 (2011) 1577-1585.

[26] M.H. Guo, Q.M. Wang, P.L. Ke, J. Gong, C. Sun, R.F. Huang, L.S. Wen, The preparation and hot corrosion resistance of gradient NiCoCrAlYSiB coatings, Surf. Coat. Technol. 200 (2006) 3942-

3949.

[27] R. Roussel, V. Kolarik, M. J. Lorenzo, H. Fietzek, Effect of Boron Addition on Micro-Aluminum-Particle-Based Multifunctional High-Temperature Coatings, Oxid. Met. 81 (2014) 179-189.

[28] J. A. Haynes, K. A. Unocic, M. J. Lance, B. A. Pint, Impact of Superalloy Composition, Bond Coat Roughness and Water Vapor on TBCs with HVOF NiCoCrAlYHfSi Bond Coatings, Surf. Coat. Technol. 237 (2013) 65-70.

[29] M. J. Maloney, Rapid Solidification Processing and Oxidation of Fine Grained Fe-Cr-Al Alloys, Ph.D. Thesis, (Massachusetts Institute of Technology, Cambridge, MA, 1989).

[30] M. J. Maloney, G. J. Yurek, Improvements in Oxidation Resistance Through Rapid Solidification Processing, In: Composites/Corrosion-Coatings of Advanced Materials, Proc. Vol. IMAM-4, S. Kimura, et al. eds., (Materials Research Society, Pittsburgh, PA, 1989) p.383.

[31] K. Onal, M. C. Maris-Sida, G. H. Meier, F. S. Pettit, Water Vapor Effects on the Cyclic Oxidation Resistance of Alumina-Forming Alloys, Mater. High Temp. 20 (2003) 327-337.

[32] J. L. Smialek, The Effect of Hydrogen Annealing on the Impurity Content of Alumina-Forming Alloys, Oxid. Met. 55 (2001) 75-86.

[33] J. L. Smialek, B. A. Pint, Optimizing Scale Adhesion for Single Crystal Superalloys, Mater. Sci. Forum 369-372 (2001) 459-466.

[34] J. Toscano, D. Naumenko, A. Gil, L. Singheiser, W. J. Quadakkers, Parameters affecting TGO growth rate and the lifetime of TBC systems with MCrAlY-bondcoats, Mater. Corros. 59 (2008) 501-507.

[35] J. Li, X. Zhang, H. Wang, M. Li, "Microstructure and mechanical properties of Ni-based composite coatings reinforced by in situ synthesized TiB_2 + TiC by laser cladding," Inter. Journal of Minerals, Metallurgy and Materials, 20 (2013) 57-64.

[36] Y. Yamamoto, G. Muralidharan, unpublished research, ORNL, 2014.

[37] J. Wang, Y. W. Chung, "Water Dissociation on Clean and Boron-Modified Single-Crystal Ni_3(Al,Ti) (110) Surfaces," J. Phys. Chem. B, 104 (2000) 3219-3223.

[38] A. N. Campbell, A. W. Mullendore, C. R. Hills, J. B. Vander Sande, "The effect of boron on the microstructure and physical properties of chemically vapour deposited nickel films," J. Mater. Sci. 23 (1988) 4049-4058.

[39] J. Doychak, M. Rühle, TEM Studies of Oxidized NiAl and Ni_3Al Cross Sections, Oxid. Met. 31 (1989) 431-452.

[40] B. A. Pint, K. L. More, Characterization of Alumina Interfaces in TBC Systems, J. Mater. Sci. 44 (2009) 1676-1686.

[41] F. S. Pettit, E. H. Randklev, E. J. Felten, Formation of $NiAl_2O_4$ by Solid State Reaction, J. Amer. Ceram. Soc., 49 (1966) 199.

[42] B.A. Pint, K.A. Unocic, J.A. Haynes, The Effect of Water Vapor Content and CO_2 on TBC Lifetime, In: D. Gandy, J. Shingledecker (Eds.), Proc. 7th Inter. Conf. on Advances in Materials Technology for Fossil Power Plants, ASM International, Materials Park, OH, 2014, pp.360-370.

[43] M. J. Lance, K. A. Unocic, J. A. Haynes, B. A. Pint, The Effect of Cycle Frequency, H_2O and CO_2 on TBC Lifetime with NiCoCrAlYHfSi Bond Coatings, Surf. Coat. Technol. in press.

Figure Captions

Figure 1. (a) Specimen mass change after 200, 1-h cycles at 1100°C in dry air or O_2, air + 10%H_2O and buffered CO_2+10%H_2O for model NiCrAl alloys and (b) parabolic rate constants from selected alloys in 100h isothermal and 200x1h cyclic tests at 1100°C in dry air, air + 10%H_2O and **90%(CO_2+0.15%O_2)+10%H_2O.**

Figure 2. Specimens mass change as function of time in 1h cycles at 1150°C in air+10%H_2O.

Figure 3. Light microscopy (a, c, e, g) and SEM BSE (b, d, f, h) images showing cross-sections of a) NiCrAl+YHfTi after 200h exposure in 0%H_2O%+Air at 1100°C and NiCrAl+YHfTiB after also after 200h exposure at 1100°C in dry air (c-d), air+10%H_2O (e-f) air+50%H_2O (g-h), and CO_2-H_2O (i-j).

Figure 4. Box and whisker plots of the measured internal oxidation for various model alloys after exposure for 200h 1h cycles without H_2O at 1100°C. Values for the alloys without B are presented for comparison [8].

Figure 5. Light microscopy of polished cross-sections after exposure for 200h at 1150°C in air+10%H_2O (a) NiCrAl+YTi (b) NiCrAl+YTiB (c) NiCrAl+YHfB; and (d) NiCrAl+YHfB in air+50%H_2O.

Figure 6. Box and whisker plots of the measured internal oxidation for various model alloys after 200, 1-h cycles in air+10%H_2O at 1150°C.

Figure 7. Light microscopy of polished cross-sections after exposure for 200h in air+10%H_2O at 1100°C a) NiCrAl+YHfTi and b) NiCrAl+YHfTiB alloys and at 1150°C c) NiCrAl+YHfTi, d) NiCrAl+YHfTiB (500h).

Figure 8. (a) EPMA backscattered electron image of NiCrAl+YHfTiB after 500h at 1150°C in air+10%H_2O and x-ray maps from the same region: (b) B and (c) Cr.

Figure 9. STEM BF cross-section images of the scale formed on a) NiCrAl+YHfB and b) NiCrAl+YHfTiB after isothermal exposure for 100h at 1100°C in **dry air**.

Figure 10. SEM secondary electron plan view images of scales formed on NiCrAl doped with YHfTi after 100h isothermal exposure at 1100°C in a) **dry air** and b) CO_2+10%H_2O and corresponding STEM HAADF images of the scales cross-section in c) **dry air** and d) CO_2+10%H_2O.

Table 1. Chemical composition in at.% determined by inductively coupled plasma and combustion analyses.

Alloy	**Ni**	**Cr**	**Al**	**Y**	**Hf**	**Ti**	**C**	**S**	**B**
NCAY	61.2	19.7	18.9	0.066	0.001	0.003	0.021	<0.0003	0.001
NCAYB	61.3	19.7	18.6	0.063	<0.001	0.003	0.038	<0.0003	0.29
NCAYTi	61.2	19.4	19.0	0.066	<0.01	0.31	0.024	<0.0003	<0.001
NCAYTiB	59.9	20.1	19.2	0.071	<0.01	0.32	0.032	<0.0003	0.25
NCAYHf	62.3	15.1	22.5	0.030	0.040	0.003	0.024	<0.0003	<0.001
NCAYHfB	60.6	16.8	22.2	0.015	0.037	<0.01	0.028	<0.0003	0.33
NCAYHfTi	61.9	15.2	22.6	0.020	0.043	0.31	0.017	<0.0003	<0.001
NCAYHfTiB	60.5	16.6	22.3	0.014	0.040	0.32	0.032	<0.0003	0.28

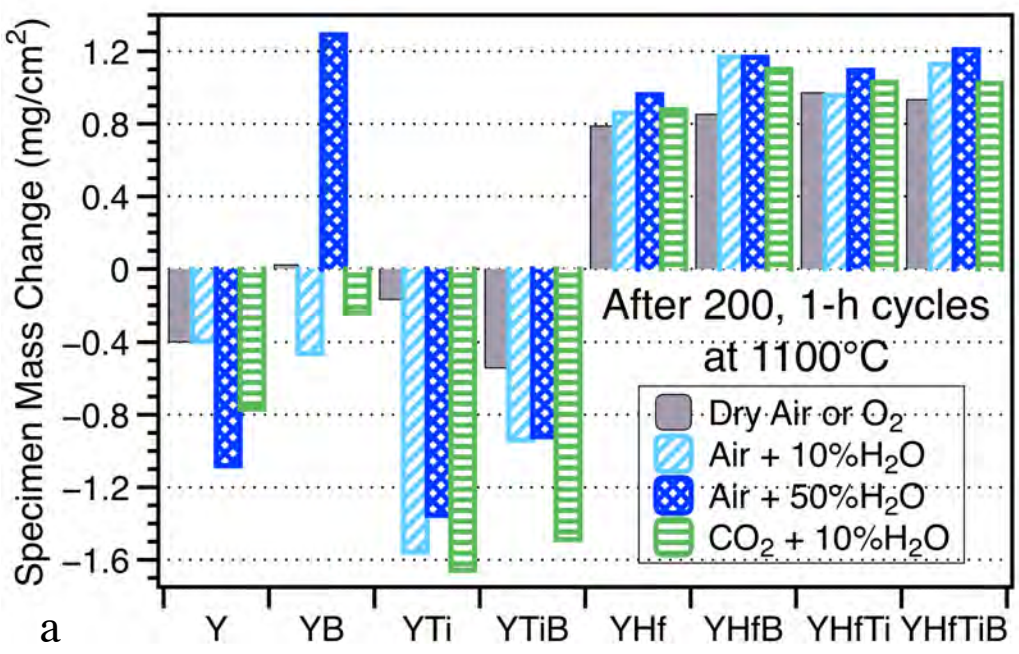

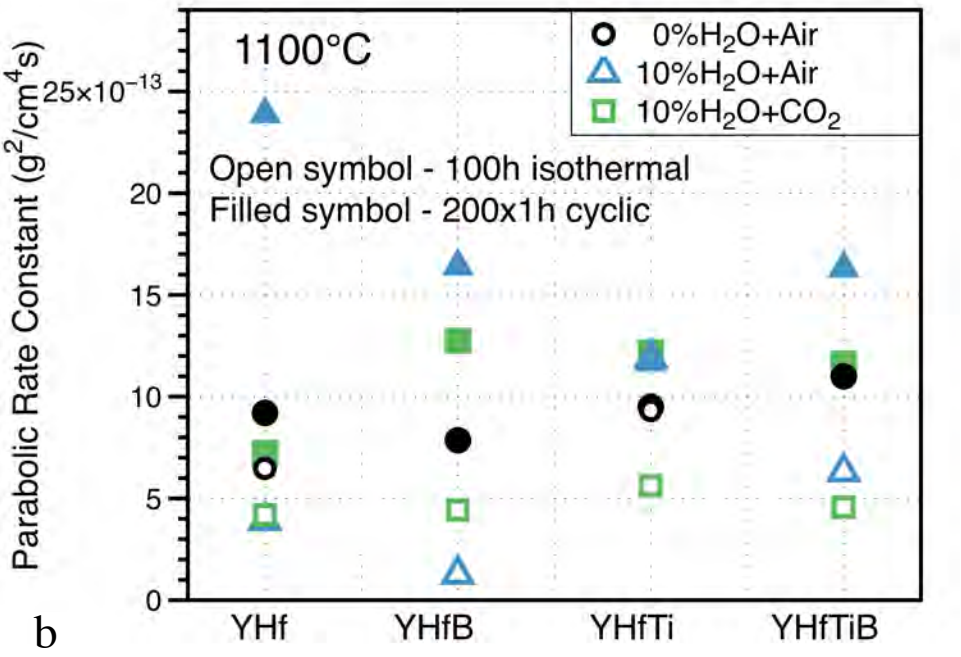

Figure 1. (a) Specimen mass change after 200, 1-h cycles at 1100°C in dry air or O_2, air + 10%H_2O and buffered CO_2+10%H_2O for model NiCrAl alloys and (b) parabolic rate constants from selected alloys in 100h isothermal and 200x1h cyclic tests at 1100°C in dry air, air + 10%H_2O and 90%(CO_2+0.15%O_2)+10%H_2O

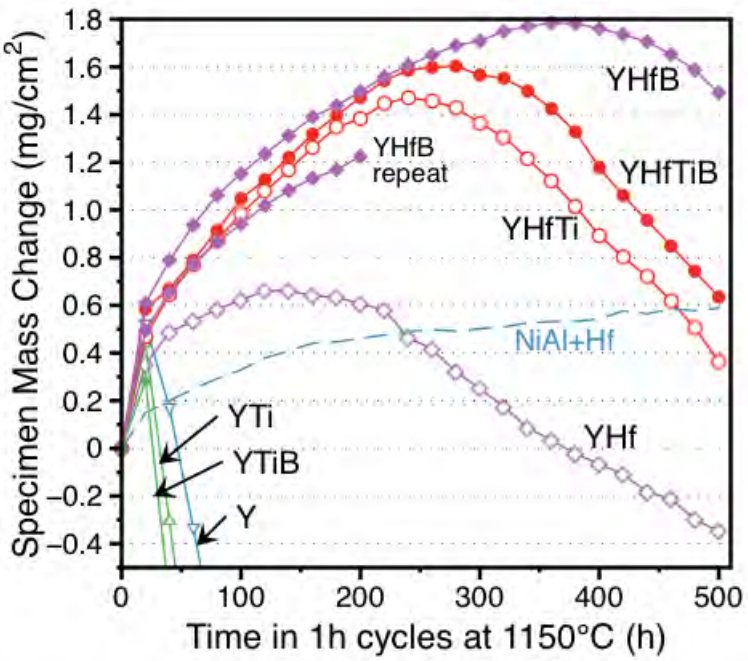

Figure 2. Specimens mass change as function of time in 1h cycles at 1150°C in air+10%H_2O.

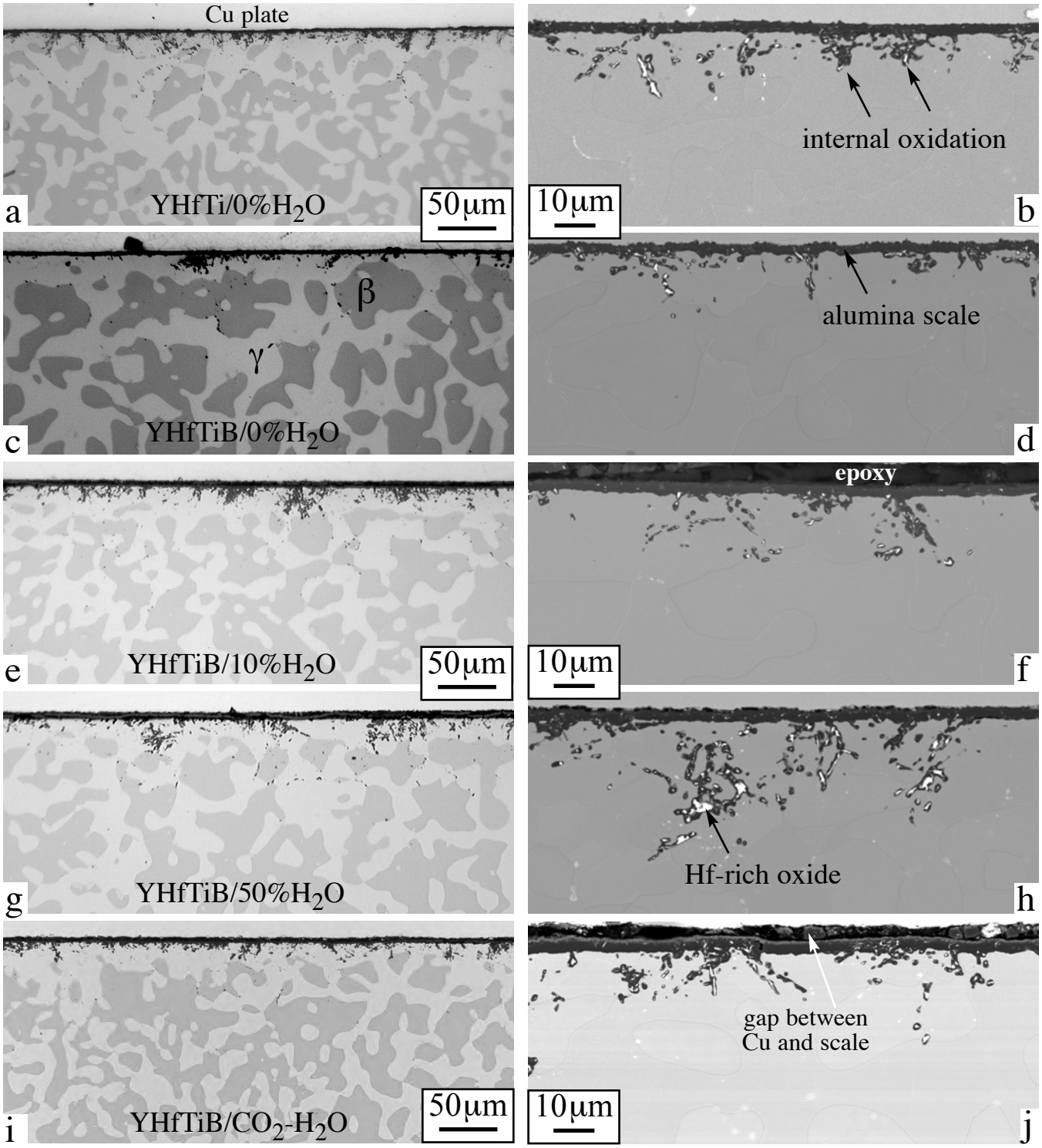

Figure 3. Light microscopy (a, c, e, g) and SEM BSE (b, d, f, h) images showing cross-sections of a) NiCrAl+YHfTi after 200h exposure in 0%H_2O%+Air at 1100°C and NiCrAl+YHfTiB after also after 200h exposure at 1100°C in dry air (c-d), air+10%H_2O (e-f) air+50%H_2O (g-h), and CO_2-H_2O (i-j).

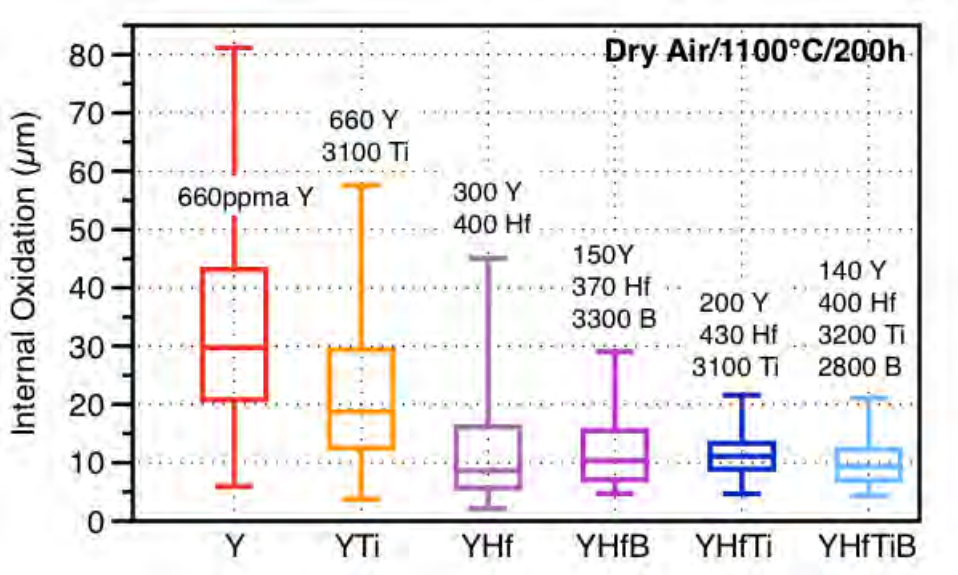

Figure 4. Box and whisker plots of the measured internal oxidation for various model alloys after exposure for 200h 1h cycles without H_2O at 1100°C. Values for the alloys without B are presented for comparison [8].

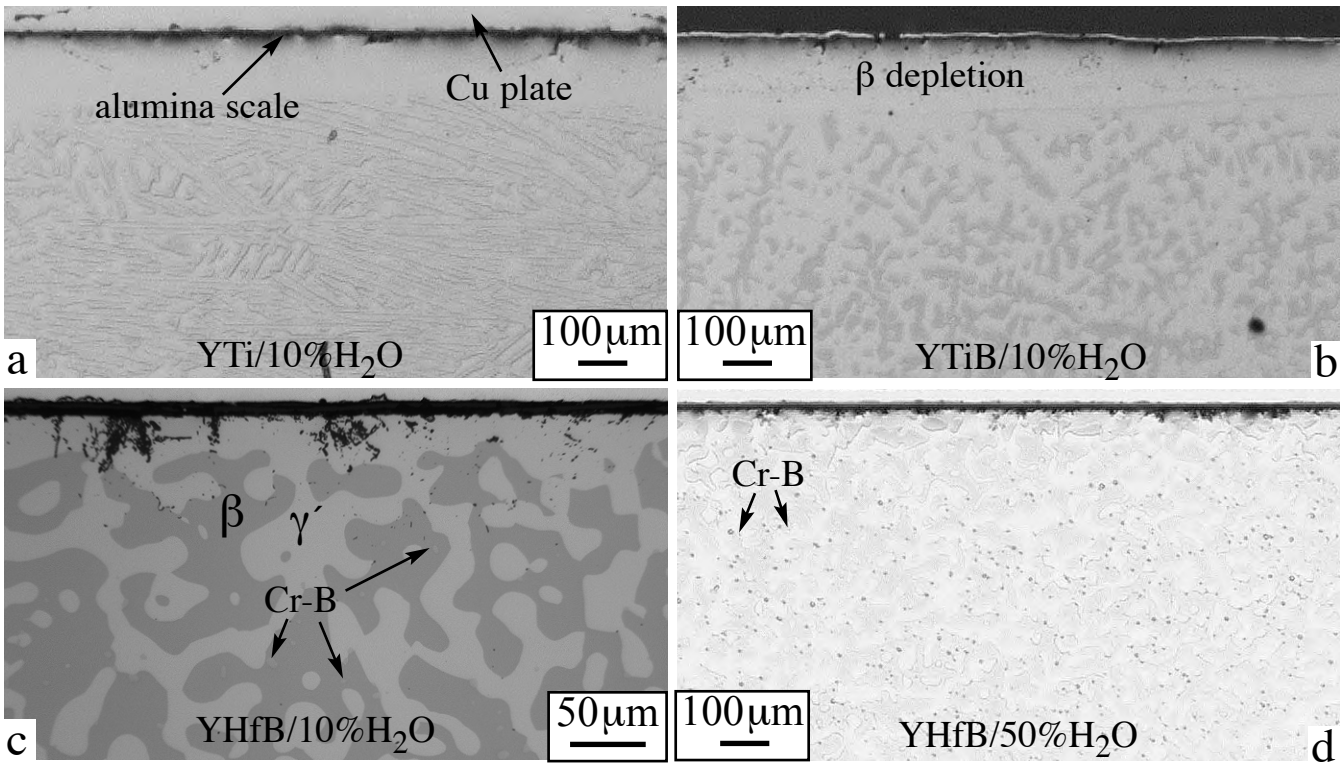

Figure 5. Light microscopy of polished cross-sections after exposure for 200h at 1150°C in air+10%H_2O (a) NiCrAl+YTi (b) NiCrAl+YTiB (c) NiCrAl+YHfB; and (d) NiCrAl+YHfB in air+50%H_2O.

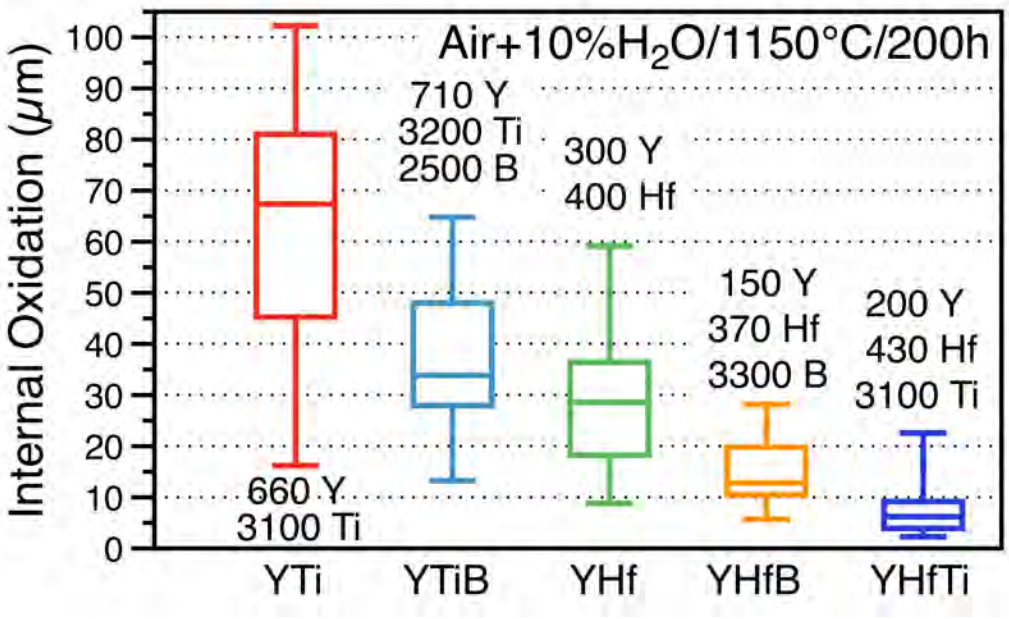

Figure 6. Box and whisker plots of the measured internal oxidation for various model alloys after 200, 1-h cycles in air+10%H_2O at 1150°C.

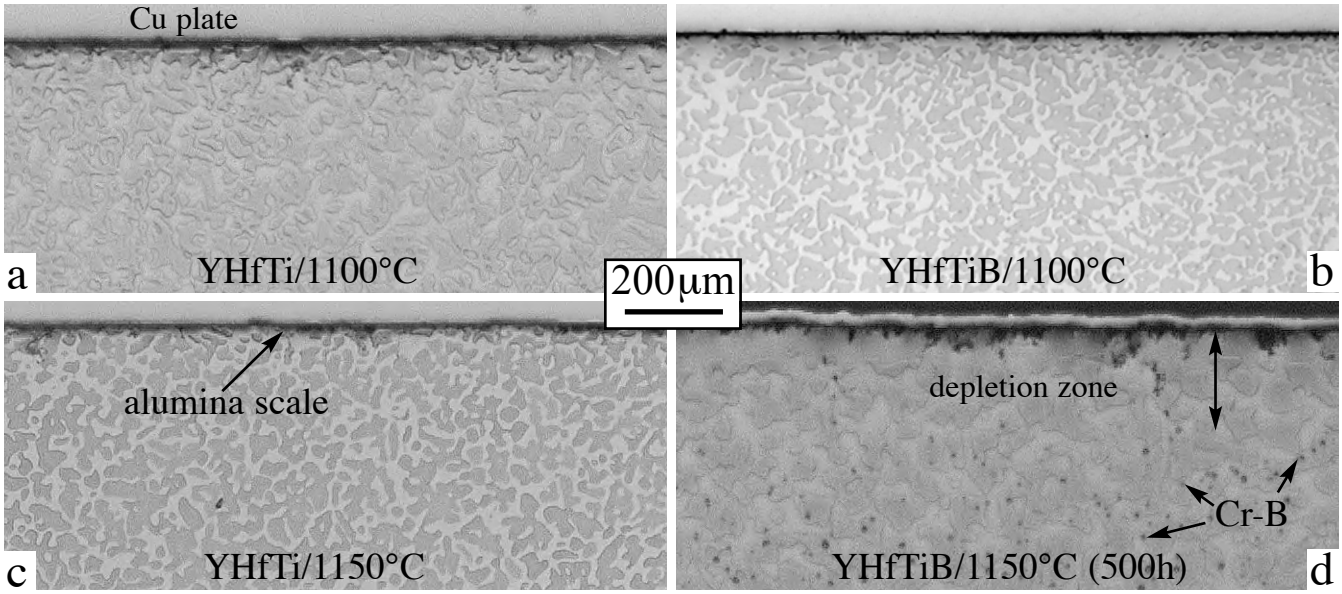

Figure 7. Light microscopy of polished cross-sections after exposure for 200h in air+10%H_2O at 1100°C a) NiCrAl+YHfTi and b) NiCrAl+YHfTiB alloys and at 1150°C c) NiCrAl+YHfTi, d) NiCrAl+YHfTiB (500h).

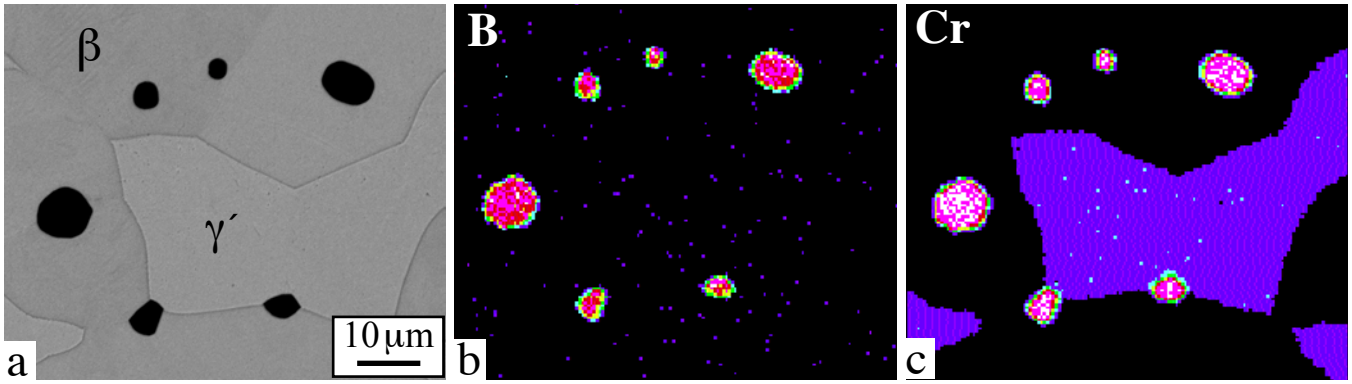

Figure 8. (a) EPMA backscattered electron image of NiCrAl+YHfTiB after 500h at 1150°C in air+10%H_2O and x-ray maps from the same region: (b) B and (c) Cr.

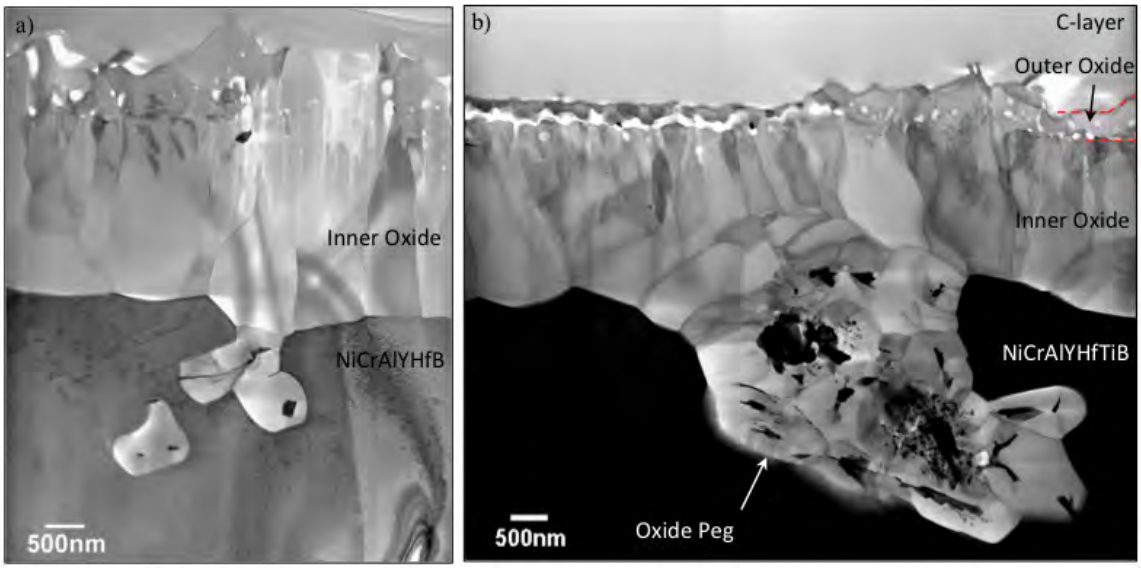

Figure 9. STEM BF cross-section images of the scale formed on a) NiCrAl+YHfB and b) NiCrAl+YHfTiB after isothermal exposure for 100h at 1100°C in dry air.

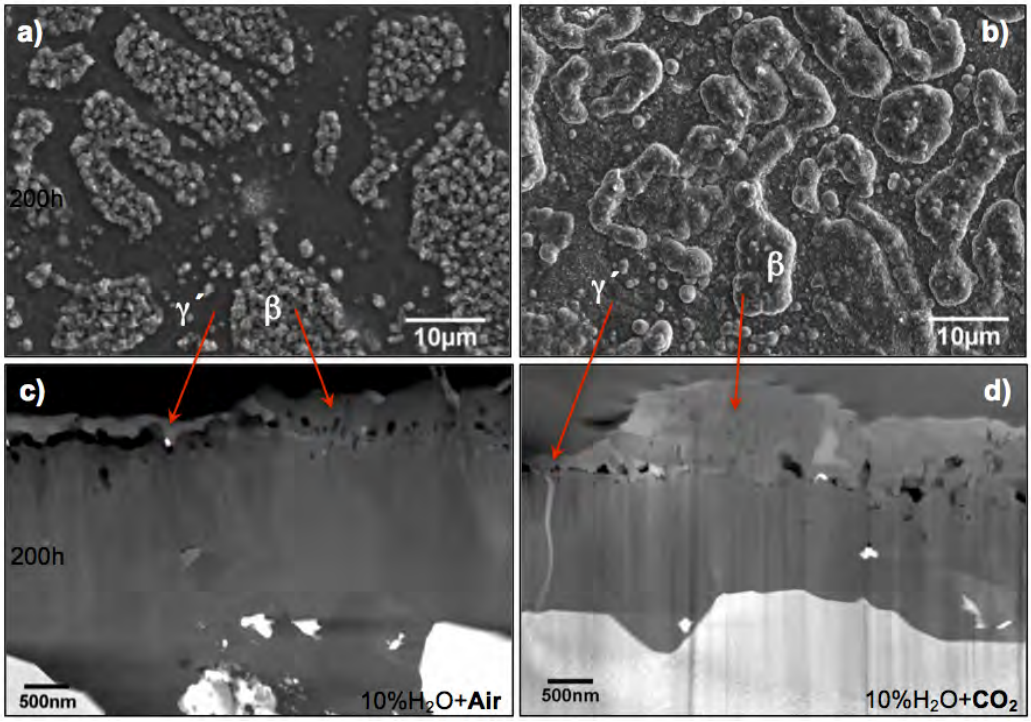

Figure 10. SEM secondary electron plan view images of scales formed on NiCrAl doped with YHfTi after 100h isothermal exposure at 1100°C in a) dry air and b) CO_2+10%H_2O and corresponding STEM HAADF images of the scales cross-section in c) dry air and d) CO_2+10%H_2O.